Ab initio lattice dynamics calculation of vibrational density of states and Raman active modes of the olivine mineral Ni_2SiO_4

2008 J. Phys.: Condens. Matter 20 285203

(http://iopscience.iop.org/0953-8984/20/28/285203)

IOP PUBLISHING JOURNAL OF PHYSICS: CONDENSED MATTER

J. Phys.: Condens. Matter **20** (2008) 285203 (7pp) doi:10.1088/0953-8984/20/28/285203

Ab initio lattice dynamics calculation of vibrational density of states and Raman active modes of the olivine mineral Ni_2SiO_4

Mohamed Zbiri[1], Tom Fennell[2], Jon W Taylor[3], Mechthild Enderle[1], Garret C Lau[4], Robert J Cava[4] and Mark R Johnson[1]

[1] Laue Langevin Institute, 38042 Grenoble Cedex 9, France
[2] London Centre for Nanotechnology, 17-19 Gordon Street, London, WC1H 0AJ, UK
[3] ISIS Facility, Rutherford Appleton Laboratory, Chilton, Didcot OX11 0QX, UK
[4] Department of Chemistry, Princeton University, Princeton, NJ 08544, USA

E-mail: zbiri@ill.fr

Received 21 April 2008, in final form 20 May 2008
Published 13 June 2008
Online at stacks.iop.org/JPhysCM/20/285203

Abstract

We present results of *ab initio* lattice dynamics calculations for the olivine mineral Ni_2SiO_4 using first-principles improved approaches within the Kohn–Sham formulation of density functional theory. Dispersion relationships, vibrational density of states and Raman shifts have been evaluated using the direct method. The calculations are compared with data from inelastic neutron scattering and Raman spectroscopy experiments. Non-spin-polarized calculations lead to clear structural instabilities and discrepancies with the measurements. Magnetic effects are taken into account by including first spin-polarization and then also a Hubbard term to describe correctly the strongly correlated character of the 3d electrons of Ni^{2+} ions. Results of these models are in excellent agreement with the observations, indicating that the structural stability and dynamics of Ni_2SiO_4 depend strongly on the magnetic interactions, spin–lattice coupling and electron correlation. These calculations will be used to help separate phonon and spin contributions in on-going studies of magnetic excitations.

(Some figures in this article are in colour only in the electronic version)

1. Introduction

Spinels are being extensively studied theoretically and experimentally to investigate and elucidate their spin–lattice coupling [1–3]. This phenomenon has implications for phase transitions and phonon spectra for a wide variety of materials including frustrated magnets [3, 4]. On the other hand olivines, which are an allotropic variety and a pressure-dependent phase of spinels, are also relevant materials for such investigations offering the possibility to gain insights into spin–lattice coupling and frustration mechanisms within a phase-dependent framework, since structural variations are involved in this case [5, 6]. Whereas spinels are composed of corner-sharing tetrahedra, olivines contain chains of corner-sharing triangles (saw-tooth chain), as observed in the orthosilicate polymorphs (M_2SiO_4, M = divalent cation), some of which are important rock forming minerals in the upper mantle of the earth [7, 8].

Generally, the olivine–spinel allotropic transformation occurs at high pressure [9]. But in the case of the mineral Ni_2SiO_4, where the olivine structure exists at atmospheric pressure, the transformation to the spinel phase is accomplished at lower pressures compared to those required for other orthosilicates with different divalent cations, for instance, forsterite Mg_2SiO_4 [5]. Thus, the mineral Ni_2SiO_4 is a good model system for the study of its lattice dynamics,

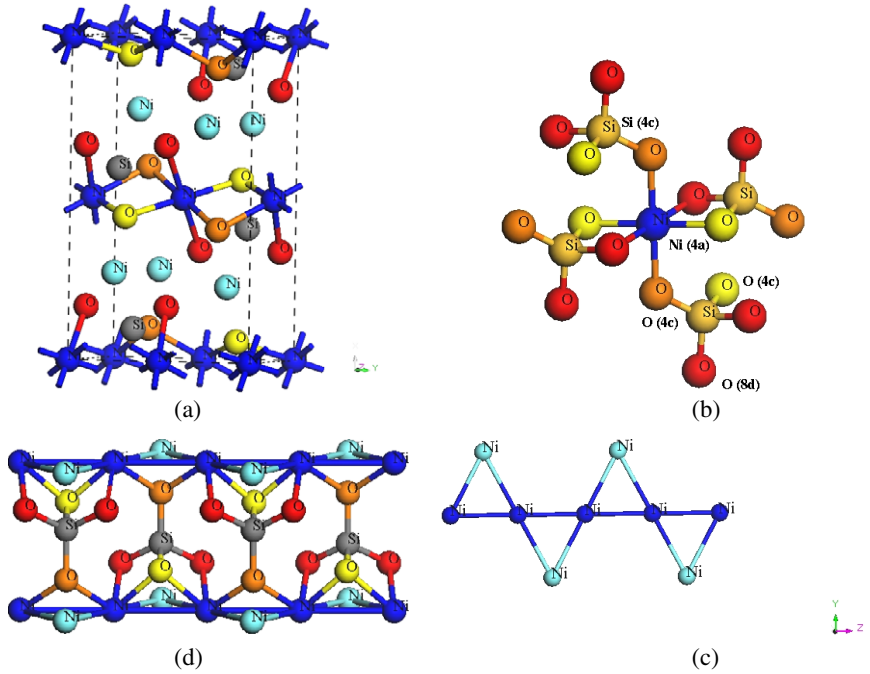

Figure 1. Schematic illustrations of the structure of Ni_2SiO_4 with views of different geometrical arrangements: (a) the unit cell, (b) NiO_6 octahedra connected to SiO_4 tetrahedra, (c) triangular geometry formed by in-chain and off-chain nickel atoms in a frustrated configuration, and (d) Nickel planes connected through SiO_4 tetrahedra. The crystallographically inequivalent positions are indicated between brackets.

which are related to the structural stability and phase transition mechanisms. Experimentally, the different structural phases of Ni_2SiO_4 and the formation of some solid solutions with other compounds have been investigated and Raman and infrared activities determined [10–12]. However, the interpretation of the corresponding modes did not consider effects of the magnetic electrons [13] of Ni^{2+} cations on lattice vibrations, and hence a possible spin–lattice coupling in this case. Recent work on geometric magnetic frustration, exploiting for the first time the chain of corner-sharing triangles (form of saw-tooth) formed by Ni^{2+} cations (see figure 1), has been reported [14]. It suggests the presence of a magnetic structure in which a sublattice possessing a spin gap interacts with surrounding local-moments of Ni^{2+} ions. The extent of frustration proposed in this work seems to be at odds with the original investigation of the magnetic structure in which a well-defined ordered magnetic phase was observed [13]. Studies of the magnetic structure and excitations are therefore on-going and a clear understanding of the phonons is required in order to separate the spin and phonon contributions to the total, inelastic neutron scattering (INS) signal.

In this context, we continue to explore the phenomenon of magneto-structural correlation and possible geometric frustration in this material by carrying out first-principles calculations to study lattice dynamics and related properties. To our knowledge, these are the first such *ab initio* simulations to be performed on Ni_2SiO_4. We note that the fayalite Fe_2SiO4, which is the end member of the olivine type silicate, has been the subject of computational study to investigate the effect of pressure on its electronic structure and magnetic properties [15, 16].

We present lattice dynamics calculations using the direct method [17] within the Kohn–Sham formulation of the density functional theory (KSDFT) [18, 19]. Vibrational density of states (vdos) together with the active Raman modes are derived and compared to experimental data. Values of Raman shifts are compared to available observed spectra from literature. Calculated total vdos are compared to our measurements from INS experiments performed at ISIS [20]. Full experimental details will not be discussed here but will be the subject of a future publication, combining NS measurements and DFT simulations, dedicated to the study of magnetic excitations and frustration in Ni_2SiO_4-olivine.

The present work has three goals: (i) show the importance of spin-polarization and electron correlation to describe the structure and dynamics of Ni_2SiO_4-olivine using accurate *ab initio* quantum modeling, (ii) from the *ab initio* simulations, extract the whole vdos spectra together with the complete number of expected Raman active modes, as predicted by group theory analysis, and; (iii) computationally investigate the observed vibrational spectrum. This paper is organized as follows: in section 2 the computational details of our calculations are summarized. The experimental data used for comparison with simulations are summarized in section 3. Sections 4 and 5 are dedicated to the presentation of the results of calculations and discussion, respectively. Finally, conclusions are drawn in section 6.

2. Computational details

Relaxed geometries and total energies were obtained using the projector-augmented wave (PAW) formalism [21] of the

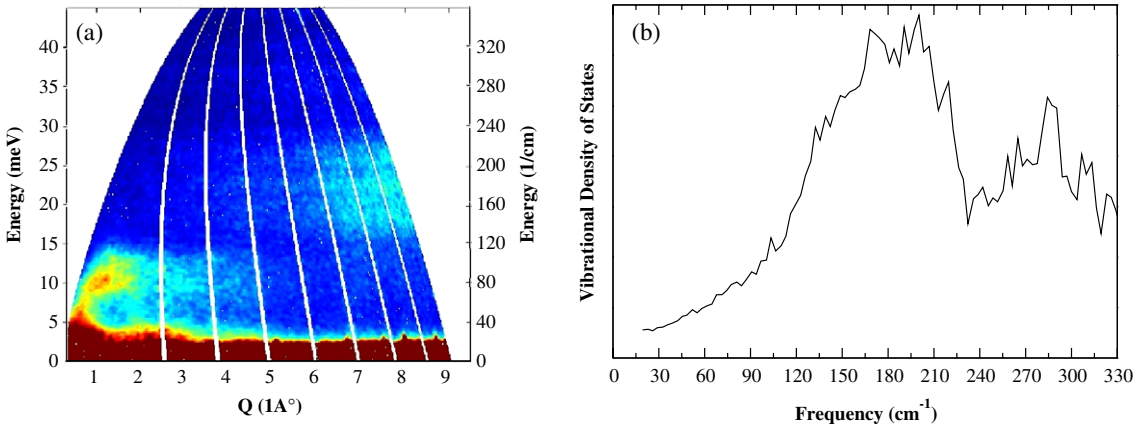

Figure 2. Measured $S(Q, \omega)$ map (a) together with a vdos (b) obtained by the summing up of intensity in the 6–9 Å^{-1} $|Q|$-range.

KSDFT [18, 19] at the generalized gradient approximation level (GGA), implemented in the Vienna *ab initio* simulation package (VASP) [22, 23]. The GGA was formulated by the Perdew–Burke–Ernzerhof (PBE) [24, 25] density functional. Non-spin-polarized calculations, spin-polarized calculations, and spin- polarized calculations with on-site Hubbard correction are three simulation types adopted throughout this work. We will refer to these models as GGA, σ-GGA, and σ-GGA + U, respectively. The on-site Coulomb interaction was accounted for in the model σ-GGA + U within the Dudarev approach [26] using $U_{\text{eff}} = U - J = 4$ eV. Calculations using different values of U were also performed while keeping J fixed at 1.0 eV [27], but only the presently reported value $U_{\text{eff}} = 4$ eV leads to a very good agreement with the experimental data (lattice parameters, vdos and Raman modes). All results converge well with respect to k-mesh and energy cutoff for the plane wave expansion. The break conditions for the self-consistent field (SCF) and for the ionic relaxation loops were set to 10^{-6} eV and 10^{-4} eV Å^{-1}, respectively. The latter break condition means that the obtained Hellmann–Feynman forces are less than 10^{-4} eV Å^{-1}.

Full geometry optimization was carried out on the experimental single cell [28] of the Ni_2SiO_4-olivine with six crystallographically inequivalent atoms, shown in figure 1. The space group is *Pnma* with four formula-units per unit cell (28 atoms). In order to describe correctly forces between neighbors and next-nearest neighbors, the supercell approach was adopted for lattice dynamics calculations to get a good estimation of force constants.

The resulting relaxed structure was then used to construct a (a, 2*b, 2*c) supercell containing 16 f.u. (112 atoms), b and c being the shorter axes. Total energies were calculated for 36 generated structures resulting from individual displacements of the six symmetry inequivalent atoms in the supercell, along the six inequivalent Cartesian directions ($\pm x$, $\pm y$ and $\pm z$). Phonons are extracted from subsequent calculations using the direct method [17] as implemented in the Phonon software [29].

3. Experimental data

A powder sample of Ni_2SiO_4 weighing ≈18.00 g was studied using the direct geometry spectrometer MARI, at ISIS, configured with a gadolinium chopper.

The data discussed here was collected at 30 K with an incident energy of 50 meV and chopper rotation frequency of 300 Hz. This gives an instrumental energy resolution of 0.6 meV (∼4.8 cm^{-1}). The intensities were normalized to correct for detector efficiencies using data recorded for a vanadium sample in the same spectrometer configuration. An absolute scale of intensity was established using data recorded for a vanadium sample with no chopper (i.e. white beam). The normalized data were corrected for the Debye–Waller and Bose factors.

Figure 2 shows the observed coherent dynamic structure factor $S(Q, \omega)$, and a vdos obtained by summing up intensity in the 6–9 Å^{-1} $|Q|$-range in the $S(Q, \omega)$ map. Interesting features are observed in the energy range 15–30 meV (∼120–240 cm^{-1}) where the phonon density of states is more pronounced than in the higher energy range 30–40 meV (∼240–320 cm^{-1}). The intensity at low $|Q|$ and low energy transfer is dominated by the magnetic excitations. The low energy part of the phonon spectrum, i.e, 5–15 meV (∼40–120 cm^{-1}), does not show any sharp peaks, characteristic of optic phonons.

Raman spectroscopy is a valuable characterization technique which allows the determination of the activity of the observed phonons, and hence which modes are of interest. It is directly related to the vibrational density of states. The complexity of the observed vibrational spectrum in this case, compared for instance to the spinel structure (higher pressure), is due to the lowering in local symmetry from the O_h (spinel phase) to the D_{2h} (olivine phase) caused by the strong pressure-dependent structural deformation.

The geometrical distortion implies a complete lifting of degeneracy in this case. Consequently, the number of Raman modes will be larger for the olivine than in the spinel case, since irreducible representations in O_h symmetry become reducible under D_{2h}. According to group theory analysis of the olivine structure, there are 36 Raman active modes.

Table 1. Available experimental data of Raman shifts cm^{-1} taken from literature. Exp1 refers to data taken from [12], Exp2a and Exp2b refer to data taken from [11].

Exp1	181	221	272	298	344	414	521	560	819	839	867	952	
Exp2a	170	185	196	255	273	299	306	322	423	467	522	559	567
	819	840	869	889	902	935	954						
Exp2b	218	250	270	292	336	416	520	557	817	836	860	885	946

Table 2. Experimental [28] and optimized lattice parameters and volumes.

	Exp	σ-GGA + U	σ-GGA	GGA
a (Å)	10.123	10.124	10.135	10.082
b (Å)	5.914	5.924	5.925	6.022
c (Å)	4.731	4.742	4.733	4.735
V (Å^3)	283	284	284	287

The corresponding reducible representation is $11A_g + 7B_{1g} + 11B_{2g} + 7B_{3g}$.

Table 1 summarizes available Raman shifts taken from literature for Ni_2SiO_4 [12, 11]. The minimal and maximal Raman shifts are 170 and 954 cm^{-1}, respectively. It can be seen that the observed number of Raman modes is far less than expected. The weakness of the signal is the crucial factor for the lack of observed bands in the vibrational spectrum of olivines [12]. This fact highlights an advantage of INS which is that there are no selection rules and all phonons are visible.

In this context, *ab initio* lattice dynamics calculations are needed to model the complete range of the expected activity together with the projected vdos in order to identify the dynamical atomic contribution to the total spectrum.

4. Results: *ab initio* modeling

Optimized lattice constants are compared to experimental values in table 2. Results of calculations using σ-GGA+U and σ-GGA models, and considering the volume, are in excellent agreement with experiment, indicating that there is a spin–lattice coupling in this case.

Spin degrees of freedom must therefore be explicitly accounted for in order to capture the correct physics of the structure. The on-site Coulomb interaction also has a considerable effect, since the derived values, using σ-GGA+U agree better with measured ones.

When adopting the GGA-only model, the relaxed structure deviates from the experimental one in such a way that the a-axis becomes shorter, and the shorter axes (b, c) are slightly elongated, giving an increase in volume. The interpretation is that spin–lattice coupling and on-site Coulomb repulsion are needed to describe and, indeed, maintain the physical structural distortion. The effect on structural stability of neglecting spin-polarization is also confirmed by lattice dynamics calculations based on the non-spin-polarized (GGA model) total energy calculations. The lack of spin degrees of freedom leads to structural instabilities as shown in the calculated vdos by a negative frequency contribution (imaginary frequencies) with unphysical dispersion relationships. This is accurately corrected by including spin-polarization (σ-GGA and σ-GGA + U) in the lattice dynamics calculations as discussed hereafter.

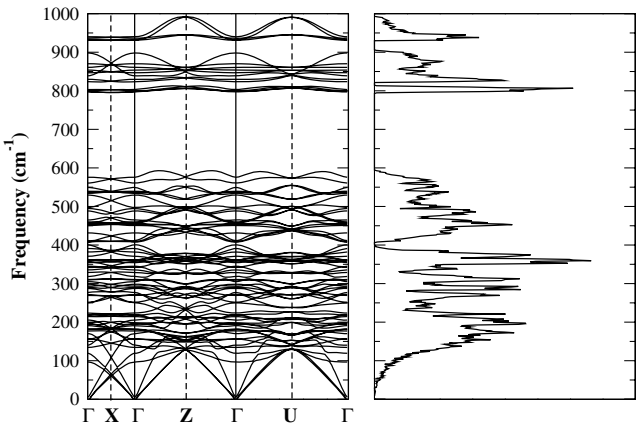

Figure 3. Calculated phonon dispersion relationships and total vibrational density of states. The Bradley–Cracknell notation is used for the high symmetry points Γ (0, 0, 0), X($\frac{1}{2}$,0, 0), Z(0, 0, $\frac{1}{2}$) and U($\frac{1}{2}$, 0, $\frac{1}{2}$).

Figure 3 shows the phonon band structure and vibrational density of states obtained using the σ-GGA + U model for geometry optimization and total energy calculation. The main features observed in the dispersion curves reveal the clear dispersive character of the bands and the presence of dense bands in the low- and mid-lying frequency ranges. This is indicative of the strong interaction of the magnetic Ni^{2+} ions with the lattice modes (nickel atoms are the heaviest species in Ni_2SiO_4). In this context, some relevant frequency ranges can be extracted for further analysis using the vdos projected into crystallographically inequivalent atoms and Raman activity, i.e; 150–400 and 420–560 cm^{-1}. We note at this point that the lowest lying optic branches have a frequency of 150 cm^{-1}, corresponding to the smoothly varying, low frequency phonon spectrum observed experimentally.

Table 3 summarizes estimated Raman active frequencies obtained by lattice dynamics simulations. Both σ-GGA and σ-GGA + U total energy calculations were carried out and the resulting values are shown. As predicted by group theory analysis, 36 active modes are obtained. The minimal and maximal Raman shifts are 132 (B_{3g}) and 928 cm^{-1} (B_{2g}) using σ-GGA, and 134 (B_{3g}) and 940 cm^{-1} (B_{2g}) using σ-GGA+U, respectively. The simulated Raman activity is consistent with the calculated vdos where no clear feature is practically found close to the acoustic modes. The next step is a validation study of the theoretical models where results of the *ab initio* calculations are compared with the experimental observations.

Table 3. Calculated Raman active modes cm^{-1} per irreducible representation of the D_{2h} symmetry.

σ-GGA	A_g	138	192	261	283	333	400	473	535	791	822	922
	B_{1g}	177	266	286	344	396	513	859				
	B_{2g}	178	224	269	289	350	399	494	543	792	825	928
	B_{3g}	132	248	295	354	416	510	853				
σ-GGA + U	A_g	140	191	272	294	342	409	497	561	798	824	932
	B_{1g}	177	269	290	354	408	539	870				
	B_{2g}	182	218	287	305	358	412	530	576	803	829	940
	B_{3g}	134	252	298	361	431	536	854				

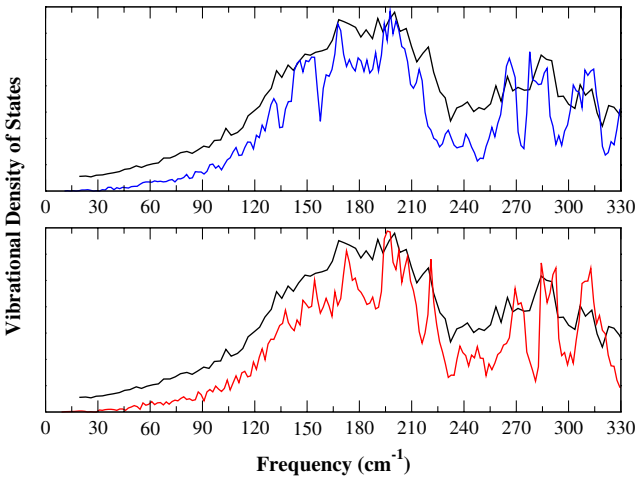

Figure 4. Experimental and calculated vdos. Simulated spectra are obtained from σ-GGA (top) and σ-GGA + U (bottom) total energy calculations, respectively.

5. Discussion: simulations versus observations

Figure 4 compares observed and simulated vdos using the total energy model calculations σ-GGA and σ-GGA+U. Although the calculations cover the whole frequency range, the spectral range in this case is restricted to a maximal value of 363 cm^{-1} (45 meV) which is within the observed limit. Very good agreement is found for both the profile of the spectra and the position of the peaks. This is indicative of the adequacy of the theoretical models. The observed features reveal that σ-GGA + U performs almost identically to σ-GGA in the low- and mid-lying part of the spectrum (120–240 cm^{-1}), whereas it agrees better in the high-lying part (240–360 cm^{-1}).

The experimental vdos shows many interesting features which are related to the observed Raman activity. In this context, clear strong peaks are observed with frequencies around 180, 210, 280, 300, and 320 cm^{-1}. All these features in the density of states seem to be Raman active when considering observed shifts, summarized in table 1.

The next step is to use simulated vdos to check the origin of these vibrational states, and whether there is a significant contribution of the saw-tooth chain, magnetic sublattice of Ni^{2+}. Deeper analysis of the most relevant density of states comes from the partial vdos (pvdos) projected onto crystallographically inequivalent sites. Here, only the σ-GGA + U total energy model calculation will be considered, as it has been shown to be slightly better than σ-GGA.

Table 4. Total bound scattering cross sections (barn), masses and their ratio used to weight the intensities of vdos.

Element	O	Si	Ni
σ	4.23	2.17	18.5
M	16	28	59
$\frac{\sigma}{M}$	0.26	0.08	0.31

Total vdos and partial vdos (pvdos) projected into crystallographically inequivalent sites (atoms) are reported in figure 5. There are two inequivalent positions for nickel atoms (4a and 4c), one silicon type (4c), and three crystallographically inequivalent oxygens (4c, 4c and 8d). It is important to note that the intensity of the pvdos of silicons is about ten orders of magnitude weaker than the others (it is amplified here for the sake of clarity), hence the main contribution to the total spectrum can be considered to originate mainly from the dynamics of nickel and oxygen sites.

Simulated vdos and pvdos are shown in figure 5. The simulated spectra are weighted by the cross sections (as seen by neutrons) and masses for each atomic species (see table 4) using the formulas: $\text{pvdos}_i = \sum_i \frac{\sigma_i}{M_i} \text{pvdos}_i^{\text{init}}$ and $\text{vdos} = \sum_i \text{pvdos}_i$ ($i = \{\text{Ni, Si, O}\}$), where $\text{pvdos}_i^{\text{init}}$ denotes the initially calculated partial vdos. Different frequency ranges are shown. The most relevant modes are in the low-lying part 0–400 cm^{-1}, which correspond to the available observed spectral range. There are peaks around 155 and 175 cm^{-1}, which are measured around 160 and 180 cm^{-1}, indicating vibrational modes of nickel sites. Close to 220 cm^{-1} there are strong and sharp peaks, experimentally observed around 215 cm^{-1}, whose vibrational densities correspond, from the simulations, to a collective mode of both crystallographically inequivalent nickel atoms. Dynamics in the range of 0–250 cm^{-1} are due mainly to Ni^{2+} ions (magnetic sites), vibrations of the off-chain nickels (4c positions) are stronger than those of the in-chain nickels (4a positions). Within the spectral range 250–400 cm^{-1}, dynamics of oxygen atoms dominates, the 8d oxygens which connect nickel to silicon are the strongest. There is also a noticeable contribution of the dynamics of nickel atoms, in-chain nickels showing a stronger vdos than the off-chain nickels. Such features are quite revealing.

The calculation shows, that the phonon dynamics in the lower and middle energy region of the measured vdos is dominated by the dynamics of the magnetic sites. The high energy part of the observed spectrum is due to vibrational motions of oxygens, especially those bridging nickels to silicons. Due to their very weak intensity, silicons are found to have a little effect on the whole observed dynamics.

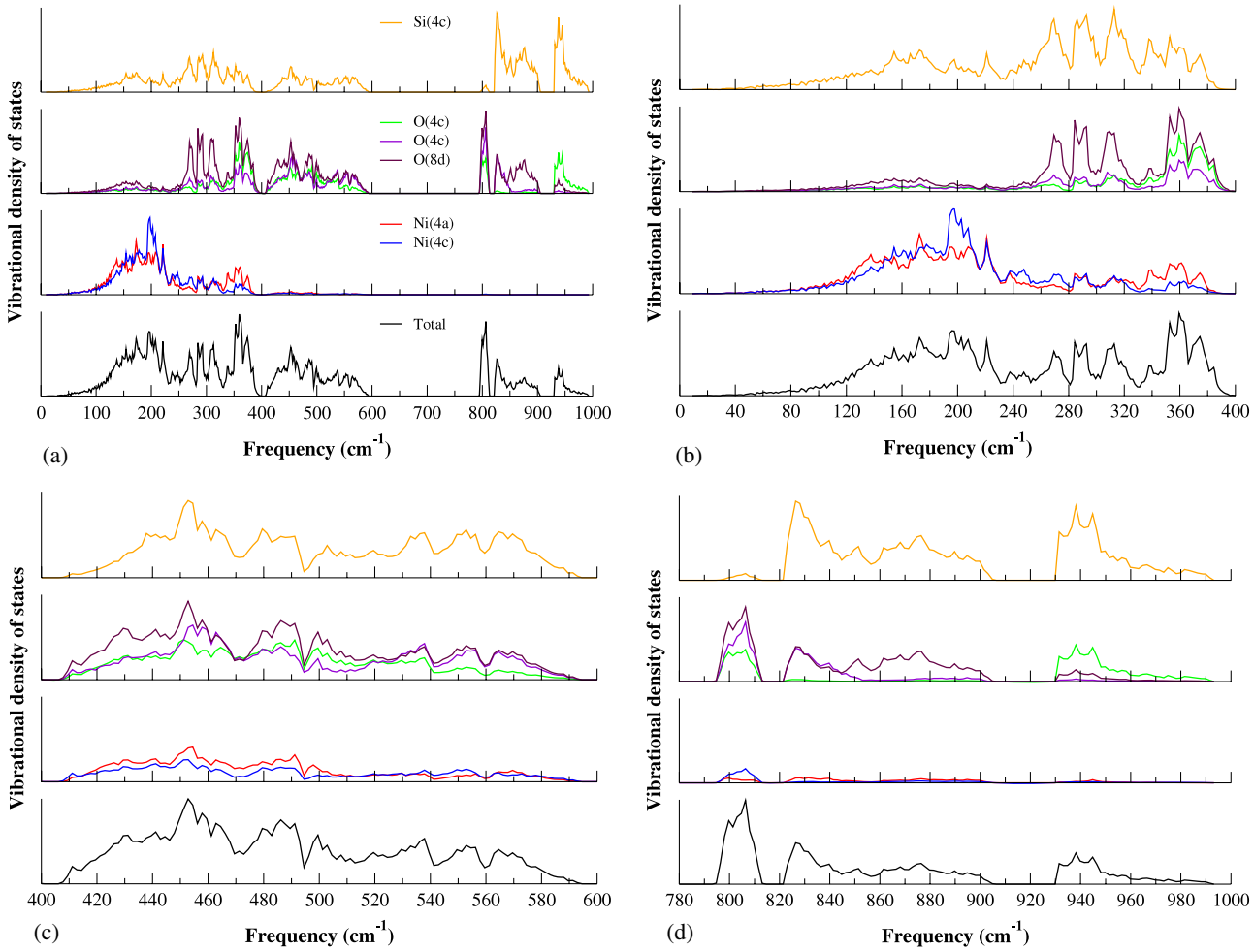

Figure 5. Pvdos projected into crystallographically inequivalent sites (σ-GGA + U model). The following frequency ranges are shown: the whole range (a), 0–400 cm^{-1} (b), 400–600 cm^{-1} (c), and 780–1000 cm^{-1} (d). Intensity of pvdos of Si atoms is the weakest, but it is amplified for the sake of clarity (see text). Colors used here do not correspond to those used in figure 2.

Simulated vdos are found to be in very good agreement with experimental data. Such agreement is also confirmed by Raman spectroscopy indicating the excellent consistency between modeling and observations as reported in figure 6. Therein simulated Raman shifts are compared with available experimental data. The corresponding numerical values are gathered in tables 3 and 1, respectively. Results of both theoretical models are in good agreement with observed Raman shifts. However, σ-GGA + U performs slightly better than σ-GGA. The observed frequency gap between ∼570 and ∼800 cm^{-1} is computationally nicely reproduced. The peaks in the experimental and simulated vdos around 160, 180 and 220 cm^{-1}, concerning the dynamics of magnetic nickel ions, are found to be Raman active.

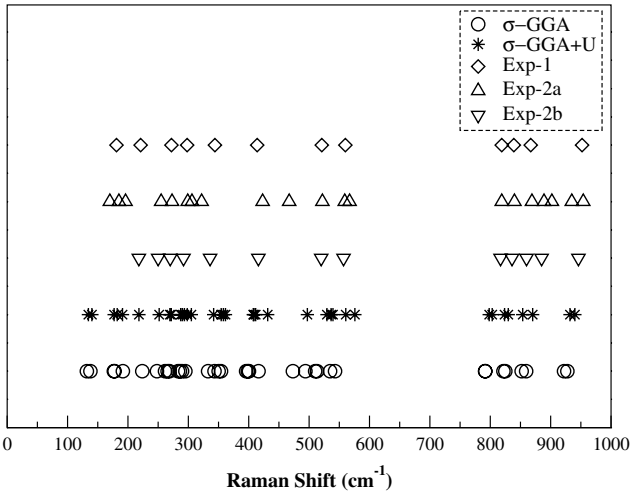

Figure 6. Calculated and available observed Raman shifts of Ni_2SiO_4.

6. Summary and perspectives

In this study, *ab initio* lattice dynamics calculations of Ni_2SiO_4-olivine are reported. The simulated vibrational density of states was compared with our inelastic neutron scattering measurements. The calculated Raman shifts were compared with available experimental data. Results of simulations are in very good agreement with observations. The analysis of the simulated data demonstrates that spin-polarization and the on-site Coulomb interaction are needed

to describe correctly the physics of this system, indicating the importance of the spin–lattice coupling and the strongly correlated character of the d-shell electrons in this case. It is found that the dynamics of the saw-tooth chain, magnetic sublattice formed by the Ni^{2+} ions dominates the observed vibrational spectrum. The two crystallographically inequivalent magnetic sites (in-chain and off-chain) having significantly different dynamics. These dynamical aspects are of considerable importance for further work using neutron scattering and *ab initio* modeling to investigate the magnetic interactions in this system. In particular, the apparent accuracy of the phonon calculation will allow us to precisely separate spin and phonon contributions in the INS signal in any region of (Q, ω) space, for powder or single crystal samples. This study will be the subject of a forthcoming publication.

References

[1] Fennie C J and Rabe K M 2006 *Phys. Rev. Lett.* **96** 205505
[2] Sushkov A B, Tchernyshyov O, Ratcliff W II, Cheong S W and Drew H D 2005 *Phys. Rev. Lett.* **94** 137202
[3] Chan K T, Sau J D, Zhang P and Cohen M L 2007 *Phys. Rev.* B **75** 054304
[4] Tchernyshyov O, Moessner R and Sondhi S L 2002 *Phys. Rev.* B **66** 064403
[5] Robie R A, Hemingway B S, Ito J and Krupka K M 1984 *Am. Mineral.* **69** 1096
[6] Gaisler S V and Kolesov B A 2007 *J. Struct. Chem.* **48** 61
[7] Burnley P C, Bassett W A and Wu T C 1995 *J. Geophys. Res.* **100** 17715
[8] Akaogi M, Ross N L, McMillan P and Navrotsky A 1984 *Am. Mineral.* **69** 499
[9] Akimoto S, Fujisawa H and Katsura T 1965 *J. Geophys. Res.* **70** 1969
[10] Tarte P and Ringwood A E 1962 *Nature* **193** 971
[11] Yamanaka T and Ishii M 1986 *Phys. Chem. Minerals* **13** 156
[12] Lin C C 2001 *J. Solid State Chem.* **157** 102
[13] Newnham R, Santoro R, Fang J and Nomura S 1965 *Acta Crystallogr.* **19** 147
[14] Hagemann I S, Khalifah P G, Ramirez A P and Cava R J 2000 *Phys. Rev.* B **62** R771
[15] Jiang X and Guo G Y 2004 *Phys. Rev.* B **69** 155108
[16] Cococcioni M, Corso A D and de Gironcoli S 2003 *Phys. Rev.* B **67** 094106
[17] Parlinski K, Li Z Q and Kawazoe Y 1997 *Phys. Rev. Lett.* **78** 4063
[18] Hohenberg P and Kohn W 1964 *Phys. Rev.* **136** B864
[19] Kohn W and Sham L J 1965 *Phys. Rev.* **140** A1133
[20] www.isis.rl.ac.uk
[21] Blöchl P E 1994 *Phys. Rev.* B **50** 17953
[22] Kresse G and Furthmüller J 1996 *Comput. Mater. Sci.* **6** 15
[23] Kresse G and Joubert D 1999 *Phys. Rev.* B **59** 1758
[24] Perdew J P, Burke K and Ernzerhof M 1996 *Phys. Rev. Lett.* **77** 3865
[25] Perdew J P, Burke K and Ernzerhof M 1997 *Phys. Rev. Lett.* **78** 1396
[26] Dudarev S L, Botton G A, Savrasov S Y, Humphreys C J and Sutton A P 1998 *Phys. Rev.* B **57** 1505
[27] Anisimov V I, Zaanen J and Andersen O K 1991 *Phys. Rev.* B **44** 943
[28] Della Giusta A, Ottonello G and Secco L 1990 *Acta Crystallogr.* B **46** 160
[29] Parlinksi K 2003 software phonon